International Journal of Fracture **76:** 373–389, 1996.

Interaction of a main crack with ordered distributions of microcracks: a numerical technique by displacement discontinuity boundary elements

ANTONIO BRENCICH and ALBERTO CARPINTERI
Department of Structural Engineering, Politecnico di Torino, C.so Duca degli Abruzzi 24, 10129 Torino, Italy

Received 5 May 1995; accepted 25 October 1995

Abstract. A boundary element technique, based on a pure displacement discontinuity formulation, is presented to solve general problems of interaction between cracks. The procedure allows detailed information and high precision at the expense of a reasonable computational effort. The comparisons with exact solutions and numerical ones for elementary case show a good performance of the method in the case of strong interacting cracks too. The interaction of a main crack with some microcrack arrays is studied in terms of amplification and shielding of the SIF at the main crack tip.

The analysis of the results shows that, while shielding can be considered a short range phenomenon, amplification has a wider range involving more distant microcracks; this fact fits well with some experimental investigations given in the literature.

1. Introduction

Experimental evidence [1–5] shows that in brittle materials a microcracked area develops in front and around a main crack tip up to quite long distances; the interaction between microcracks and between microcracks and main crack, results in a macroscopic toughening of the material. This fact gives rise to a specific interest in the interaction mechanisms, which in some cases lead to values of the SIF at the main crack tip higher than the one expected for the undamaged material, in other cases to much lower values.

Simple cases of interaction of a main crack with few microcracks have been studied by means of a point source representation of the microcracks [6] and complex potentials [7, 8] of a superposition scheme known as '*method of pseudotractions*' [9, 10] or of edge dislocation methods [11]. A small number of microcracks has been involved, usually no more than three microcracks were considered, but for periodic arrays of collinear or transversal microcracks.

The main difficulty to overcome consists of the high computational effort that is required to solve the elastic problem in the general case where weak interactions as well as strong ones can be equally expected.

Finite element simulations [14, 15] have to face heavy computational problems connected with the discretization of the continuum into finite elements, particularly when some cracks propagate, thus changing the interior boundaries of the solid.

An approximate method of analysis has been developed [12, 13] to deal with both two- and three-dimensional microcrack arrays of arbitrary geometry. The procedure, suitably proposed to be developed into an automatic code, gives good results in the case of weak interaction but leads to somewhat higher errors in the case of strong interaction at short distances.

The present work develops a numerical technique based on displacement discontinuity boundary elements which allows for considering arbitrary two-dimensional geometries of

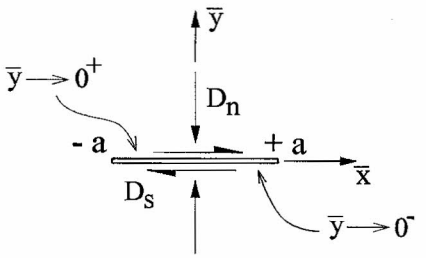

Figure 1. Displacement discontinuities along a straight segment.

microcracks with quite small errors up to very close distances between the cracks. After a comparison with results for simple cases found in the literature, more complex distributions of microcracks are considered with particular regard to the range at which interaction can be considered negligible.

2. The numerical procedure

Let us consider a two-dimensional domain, consisting of a linear elastic and isotropic material, and impose constant displacement jumps in the displacement field in the normal n and shear s direction along a segment $|\overline{x}| \leqslant a$ (Figure 1).

The displacement field is thus continuous all over the domain except for the segment $|\overline{x}| \leqslant a$ itself, where displacements are discontinuous and the quantities

$$\begin{aligned} D_n &= u_n^- - u_n^+, \\ D_s &= u_s^- - u_s^+, \end{aligned} \tag{1}$$

are called displacement discontinuities in the normal and shear direction, where u_n^+, u_s^+ and u_n^-, u_s^- are the displacements respectively of the positive ($\overline{y} \to 0^+$) and negative ($\overline{y} \to 0^-$) side of the segment with regard to the local reference system of Figure 1.

It is possible [16, 17] to express the displacement and stress fields in any point Q of the domain as a linear combination of the displacement discontinuities D_n and D_s

$$\begin{aligned} u_{\overline{x}} &= \overline{f}_{xn}(\overline{x}, \overline{y}, a) D_n + \overline{f}_{xs}(\overline{x}, \overline{y}, a) D_s, \\ u_{\overline{y}} &= \overline{f}_{yn}(\overline{x}, \overline{y}, a) D_n + \overline{f}_{ys}(\overline{x}, \overline{y}, a) D_s, \end{aligned} \tag{2}$$

$$\begin{aligned} \sigma_{\overline{xx}} &= \overline{g}_{xxn}(\overline{x}, \overline{y}, a) D_n + \overline{g}_{xxs}(\overline{x}, \overline{y}, a) D_s, \\ \sigma_{\overline{yy}} &= \overline{g}_{yyn}(\overline{x}, \overline{y}, a) D_n + \overline{g}_{yys}(\overline{x}, \overline{y}, a) D_s, \\ \tau_{\overline{xy}} &= \overline{g}_{xyn}(\overline{x}, \overline{y}, a) D_n + \overline{g}_{xys}(\overline{x}, \overline{y}, a) D_s, \end{aligned} \tag{3}$$

where the coefficients $f_{qs}(\overline{x}, \overline{y}, a)$ and $g_{qrs}(\overline{x}, \overline{y}, a)$ are functions of the co-ordinates of the point $Q(\bar{x}, \bar{y})$ and of the half-length a of the segment, whatever the loading and boundary conditions are.

Let us consider now two sets of displacement discontinuities applied to two different segments, as represented in Figure 2.

According to (2) and (3), it is possible to express the displacements and stresses in the centre of the ith segment due to displacement discontinuities applied over the jth segment

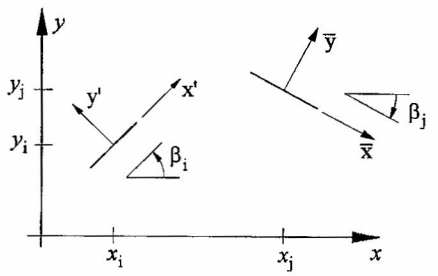

Figure 2. Two different segments over which two different sets of displacement discontinuities are imposed.

with regard to the local reference system $\overline{x}, \overline{y}$ of the same element; let these displacements and stresses be $u^i_{\overline{x}}$, $u^i_{\overline{y}}$ and $\sigma^i_{\overline{xx}}$, $\sigma^i_{\overline{yy}}$, $\tau^i_{\overline{xy}}$. A rotation of the $\overline{x}, \overline{y}$ system by an angle $\gamma = \beta_i - \beta_j$ turns the same system into the x', y' one, so that it is possible to express the displacements and stresses in the centre of the ith segment with reference to the local x', y' system. Considering that the displacement in the y' direction can be interpreted as a displacement in the normal direction, and similarly for the displacement in the x' direction and for the stresses, we can write

$$\begin{aligned} u^i_{x'} &= u^i_s = h_{xn}(\overline{x}_i, \overline{y}_i, a_i) D^j_n + h_{xs}(\overline{x}_i, \overline{y}_i, a_i) D^j_s, \\ u^i_{y'} &= u^i_n = h_{yn}(\overline{x}_i, \overline{y}_i, a_i) D^j_n + h_{ys}(\overline{x}_i, \overline{y}_i, a_i) D^j_s, \end{aligned} \tag{4}$$

$$\begin{aligned} \sigma^i_{y'y'} &= \sigma^i_n = e_{yyn}(\overline{x}_i, \overline{y}_i, a_i) D^j_n + e_{yys}(\overline{x}_i, \overline{y}_i, a_i) D^j_s, \\ \tau^i_{x'y'} &= \tau^i_s = e_{xyn}(\overline{x}_i, \overline{y}_i, a_i) D^j_n + e_{xys}(\overline{x}_i, \overline{y}_i, a_i) D^j_s. \end{aligned} \tag{5}$$

As a consequence of the physical meaning of (4) and (5), the coefficients $h_{qs}(\overline{x}_i, \overline{y}_i, a_i)$ and $e_{qrs}(\overline{x}_i, \overline{y}_i, a_i)$ represent influence coefficients, so that (4) and (5) can be rewritten in the form

$$u^i_n = E^{ij}_{nn} D^j_n + E^{ij}_{ns} D^j_s, \qquad u^i_s = E^{ij}_{sn} D^j_n + E^{ij}_{ss} D^j_s, \tag{6}$$

$$\sigma^i_n = F^{ij}_{nn} D^j_n + F^{ij}_{ns} D^j_s, \qquad \tau^i_s = F^{ij}_{sn} D^j_n + F^{ij}_{ss} D^j_s, \tag{7}$$

E^{ij}_{qr} and F^{ij}_{qr} being the *influence coefficients*.

In the case where there were m segments over which displacement discontinuities are imposed, either linked or separate from each other, the global effect on the ith segment can be obtained as superimposition of the effects of any single segment, including the ith one, thus obtaining the following expressions

$$u^i_n = \sum_{j=1}^{m} E^{ij}_{nn} D^j_n + \sum_{j=1}^{m} E^{ij}_{ns} D^j_s, \qquad u^i_s = \sum_{j=1}^{m} E^{ij}_{sn} D^j_n + \sum_{j=1}^{m} E^{ij}_{ss} D^j_s, \tag{8}$$

$$\sigma^i_n = \sum_{j=1}^{m} F^{ij}_{nn} D^j_n + \sum_{j=1}^{m} F^{ij}_{ns} D^j_s, \qquad \tau^i_s = \sum_{j=1}^{m} F^{ij}_{sn} D^j_n + \sum_{j=1}^{m} F^{ij}_{ss} D^j_s. \tag{9}$$

Any structural problem can thus be described by congruence and equilibrium equations like (8) and (9) which constitute a system of linear algebraic equations since the index i can

vary over the range $[1, m]$ of all the segments. The terms on the left-hand side of (8) and (9) represent the resulting effect, displacement or stress, due to all displacement discontinuities applied, thus representing the boundary conditions given over each segment.

If only kinematic boundary conditions are given, then the elastic problem is represented by equations like (8), while static conditions lead to a solving system like (9). If the elastic problem provides mixed boundary conditions, kinematic ones on a part of the boundary and static ones on the remaining part; the solving system will be obtained, choosing segment by segment the appropriate equations of type (8) or (9). The solution of a general problem will be provided by a system of linear algebraic equations like

$$d_n^i = \sum_{j=1}^{m} G_{nn}^{ij} D_n^j + \sum_{j=1}^{m} G_{ns}^{ij} D_s^j, \qquad d_s^i = \sum_{j=1}^{m} G_{sn}^{ij} D_n^j + \sum_{j=1}^{m} G_{ss}^{ij} D_s^j. \tag{10}$$

The displacement discontinuities D_n^j and D_s^j of (10) are in fact unknown, since the left-hand side of the system is made up of known terms (the given conditions on the boundary); the system (10) consists of $2m$ equations in $2m$ unknowns and can thus be solved.

Once the displacement discontinuities are known, stresses and displacements in any point $Q(x_Q, y_Q)$ of the continuum can be evaluated through (8) and (9) after recalculating the influence coefficients.

Finally, replacing (4) into the definition of strain for infinitesimal displacements

$$\varepsilon_{hk} = \tfrac{1}{2}(u_{h,k} + u_{k,h}), \tag{11}$$

the following expressions of the strain field can be obtained

$$\varepsilon_{xx} = u_{x,x} = \sum_{i=1}^{m} \left(\frac{\partial h_{xn}^i(x_Q, y_Q, a_i)}{\partial x} D_n^i + \frac{\partial h_{xs}^i(x_Q, y_Q, a_i)}{\partial x} D_s^i \right), \tag{12a}$$

$$\varepsilon_{yy} = u_{y,y} = \sum_{i=1}^{m} \left(\frac{\partial h_{yn}^i(x_Q, y_Q, a_i)}{\partial y} D_n^i + \frac{\partial h_{ys}^i(x_Q, y_Q, a_i)}{\partial y} D_s^i \right), \tag{12b}$$

$$\begin{aligned} \varepsilon_{xy} = \tfrac{1}{2}(u_{x,y} + u_{y,x}) = {} & \frac{1}{2} \sum_{i=1}^{m} \left(\frac{\partial h_{xn}^i(x_Q, y_Q, a_i)}{\partial y} D_n^i + \frac{\partial h_{xs}^i(x_Q, y_Q, a_i)}{\partial y} D_s^i \right) + \\ & + \frac{1}{2} \sum_{i=1}^{m} \left(\frac{\partial h_{yn}^i(x_Q, y_Q, a_i)}{\partial x} D_n^i + \frac{\partial h_{ys}^i(x_Q, y_Q, a_i)}{\partial x} D_s^i \right). \end{aligned} \tag{12c}$$

3. Modelling the cracks

Let us now consider a crack and imagine the crack line divided into a series of m straight segments over which a constant displacement discontinuity is imposed in order to model the effective profile of the crack faces. Figure 3 represents a single crack loaded in mode I which is modeled with $m = 5$ segments.

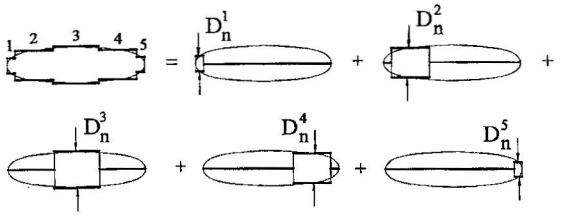

Figure 3. Discretization of a crack with $m = 5$ displacement discontinuity segments.

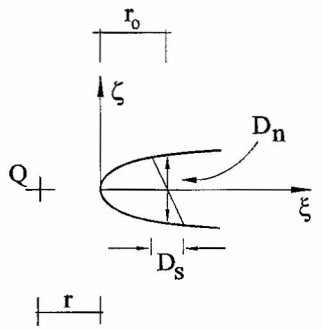

Figure 4. Displacement discontinuity (parabolic) at the crack tip.

The global problem can thus be divided into m subproblems, each consisting of a displacement discontinuity imposed on one segment on the crack line while no displacement discontinuity is imposed on the other segments (Figure 3). The stress and displacement fields can thus be obtained by summing up the contributions of all the m subproblems as resulting from (8) and (9).

The opposite faces of the crack present a parabolic deformation which is well approximated by the series of constant displacement discontinuities only in the central part of the crack, while the crack tips need to be modeled through segments on which displacements are allowed to take a parabolic shape.

With reference to Figure 4, the displacement jump from one face to the other is assumed to vary according to the law

$$u_i(\xi) = D_i\sqrt{\frac{\xi}{a_i}}, \quad i = n, s. \tag{13}$$

It can be proved that the *element self-effect*, or the effect of the displacement discontinuities over the same segment, are decoupled, as shown by the following general expressions

$$\begin{aligned}
\sigma_n^i(\overline{x}, 0) &= \frac{-G}{2\pi(1-\nu)} \lim_{\overline{y}\to 0} \int_0^{2a} u_n(\xi) \frac{1}{(x-\xi)^2 + \overline{y}^2}\, \mathrm{d}\xi, \\
\tau_s^i(\overline{x}, 0) &= \frac{-G}{2\pi(1-\nu)} \lim_{\overline{y}\to 0} \int_0^{2a} u_s(\xi) \frac{1}{(x-\xi)^2 + \overline{y}^2}\, \mathrm{d}\xi.
\end{aligned} \tag{14}$$

Substituting (13) into (14), and carrying out the integrals, the proper influence coefficients to substitute in the system (10) can be found.

Except for pressurised cracks, the boundary conditions relative to the crack segments to impose on the left-hand side of the solving system (10) are that the crack faces are stress free.

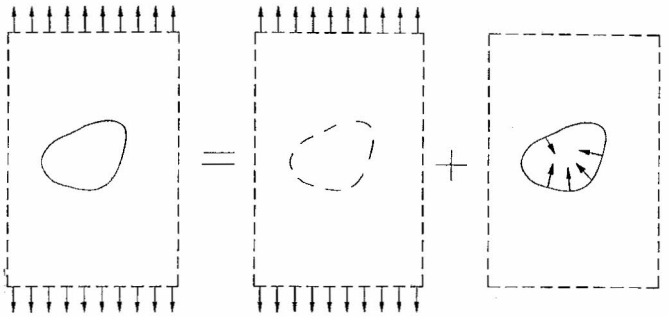

Figure 5. Decomposition of the original problem loaded at the infinity into two sub-problems.

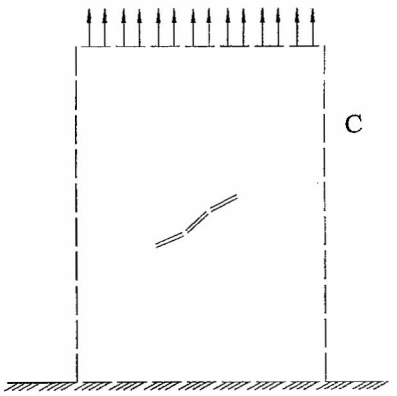

Figure 6. Finite plate discretization: external boundaries and internal contours (crack).

4. Loading conditions in an infinite plate

Let the crack represented in Figure 3 be embedded in an infinite two-dimensional domain loaded at the infinity by uniform stresses σ^{∞} and τ^{∞}. The direct application of (10), considering that the crack faces are stress free and that the corresponding terms d_n^i and d_s^i are thus zero, would lead to an homogeneous system with maximum characteristic of the coefficient matrix. The solution will be the trivial one, with no physical meaning.

Being the linear problem, it can be divided into two sub-problems: (1) the infinite domain is loaded at infinity by the applied (uniform) stresses and does not contain any crack; (2) the infinite plate has no load at infinity and the crack faces are loaded by the opposite of the stresses which result in the first subproblem along the crack lines. This procedure, which is applicable to any distribution of cracks and/or voids, is represented in Figure 5.

5. Modelling finite plates

The numeric procedure described can be straightforward applied to a finite domain.

Let us consider a sequence of M segments, forming a closed contour C, for example a rectangle ($M = 4$) as represented in Figure 6.

Suppose that the loads are uniform stresses applied over one side, the adjacent being stress free while the last side is totally constrained. In this case the solving system (10) will be made up of two sets of equations: $2m$ equations like (9) describing the equilibrium on the

Figure 7. Collinear microcrack.

crack faces, and $2M$ equations imposing the conditions on the finite boundary, part like (8) for the constrained side, and like (9) for the remaining part, expressing the stress free or the loading conditions. The known terms of the system (10) are thus the applied loads (expressing the stress free condition on the crack faces) and will be different from zero. In this way the system (10) gives, as results, the displacement discontinuities on the cracks as well as on the boundary. The last have no direct physical meaning. The absolute displacements on the boundaries can be derived from the displacement discontinuities, see equations like (1).

6. Stress intensity factors computation

Once the displacement discontinuities are known, the SIFs can be directly evaluated through the following expressions [18]

$$K_{\mathrm{I}} = D_n(r)\frac{E}{4}\sqrt{\frac{\pi}{2r}}, \qquad K_{\mathrm{II}} = D_s(r)\frac{E}{4}\sqrt{\frac{\pi}{2r}}, \tag{15}$$

where $D_n(r)$ and $D_s(r)$ are the displacement discontinuities at distance r from the crack tip, and E is the Young's modulus of the material. Since the displacement discontinuities are known directly from the system (10) in the midpoints of the segments, then the distance r in (15) is usually taken as the half-length of the segment itself.

7. Test problems

7.1. The collinear microcrack

The test case for the numerical procedure outlined in the previous section is the interaction of a main crack with a collinear microcrack (Figure 7).

This is a typical geometry inducing an amplification on the main crack, which becomes stronger as the microcrack approaches the main crack. At very short distances δ, the SIF at the main crack tip becomes some two-three times the expected value in the absence of the minor crack; short range effects are the most challenging for any numerical analysis.

We computed the SIF at the main crack tip for several distances δ, from the minimum value of $\delta/l = 0.01$ up to the maximum value of $\delta/l = 3.6$. The results are compared with the exact closed form solution obtained by Rose [6] and the approximate solution given by Gong and Horii [10] in the whole range (Figure 8), and with the solutions proposed by Rubinstein [7] and by Kachanov and Montagut [13] at very short distances (Figure 9).

It can be seen that the numerical solution fits quite well the exact results up to a very close distance. The error does not exceed 4 percent up to a distance which is 1 percent of the microcrack full-length. This good performance is obtained at the cost of a certain computational effort, but it has to be said that seldom are such severe interactions to be expected.

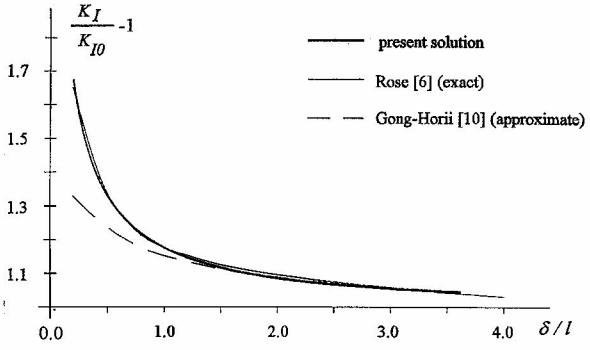

Figure 8. Comparison of the obtained diagram with the exact [6] and approximate [10] solutions.

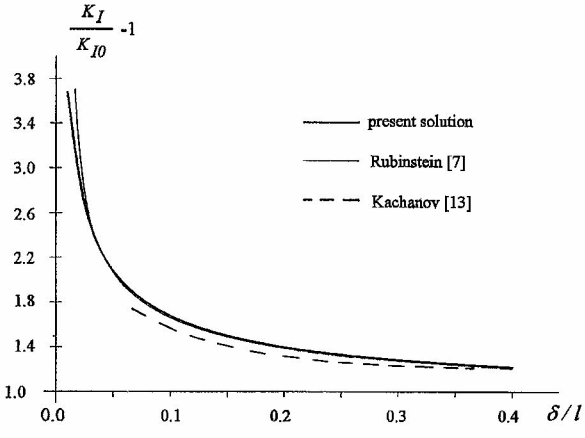

Figure 9. Comparison with further approximate results.

7.2. TWO SYMMETRICAL MICROCRACKS

The geometry represented in Figure 10 produces both amplification and shielding according to the distance d of the microcracks with respect to the main crack.

Several analyses were carried out with various values of the parameter d/l keeping the vertical distance h constant and equal, in turn, to 0.5, 1.0, 1.5 and 2.0 times the microcrack half-length l.

Figure 11 presents the diagram obtained for a vertical distance $h/l = 0.5$ and compares it to the results reported by Kachanov and Montagut [13], Rubinstein and Choi [8].

Figure 12 shows an analogous comparison, for the case $h/l = 2.0$, with the results obtained by [8] in the case of an infinite vertical stack of microcracks.

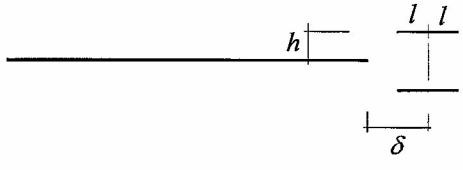

Figure 10. Two symmetrical microcracks.

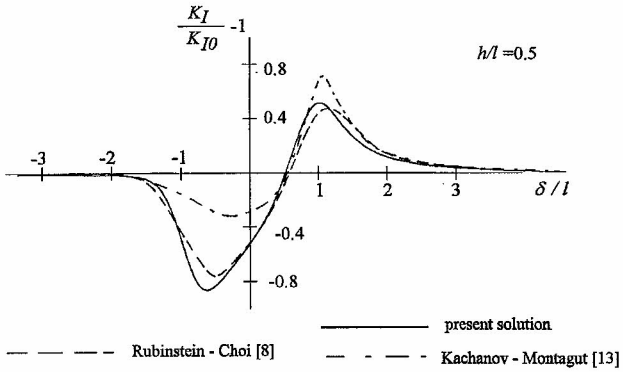

Figure 11. Numerical data from the proposed technique for the case $h/l = 0.5$, and comparison with other authors, [8], [13] and [19].

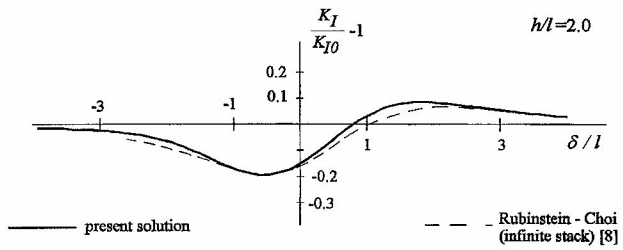

Figure 12. Results for the case $h/l = 2.0$ and comparison with other similar results [8].

Figures 11 and 12 point out a good agreement of the numerical solution with some results [8] but, in some cases, quite a significant difference from other solutions [13]. This is due to some improvements of the present technique if compared with the *pseudo-traction method* [12] as will be discussed in the concluding section. The difference with other authors is significantly small: the maximum shielding effect is here evaluated as being 84 percent of the unaffected value, while Rubinstein and Choi [8] give the estimate of 77 percent, which is quite a good agreement for such strong interactions.

Figure 13 reveals that the phenomenon is qualitatively affected by the parameter d, whereas the vertical distance h produces only quantitative changes in the amount of shielding or amplification.

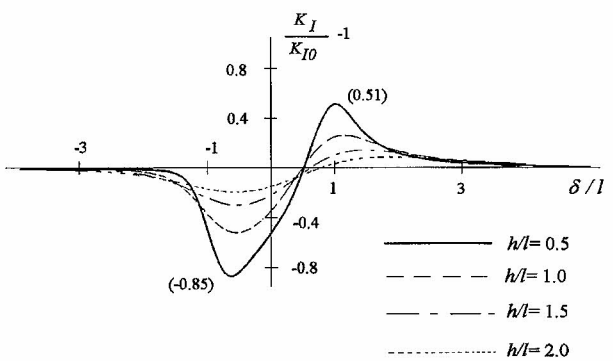

Figure 13. Diagrams for various vertical spacings.

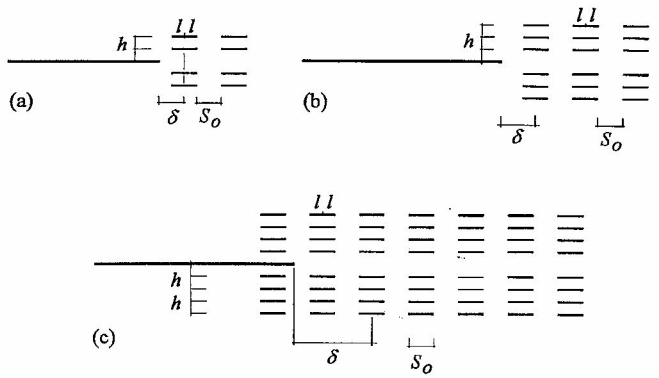

Figure 14. Three kinds of geometric distributions of microcracks: (a) 8 microcracks; (b) 18 microcracks; (c) 56 microcracks.

8. Interaction of the main crack with ordered distributions of microcracks

Different distributions of microcracks can be obtained as extensions of the previous elementary case of two symmetrically disposed microcracks.

Three kinds of geometries are considered (Figure 14):

(a) with eight microcracks, parallel to the main crack and symmetric to it;
(b) with eighteen microcracks, disposed on three columns and six rows (three on each side of the main crack);
(c) with fifty-six microcracks distributed on seven columns and four rows on each main crack side.

The geometric parameters needed to describe each geometry, normalised by the microcrack half-length, are the vertical, h, and horizontal, S_0, spacings between microcracks, and the frontal distance d of a reference column from the main crack tip. Varying the two spacings, more dense or more disperse distributions of microcracks are obtained, from which stronger or weaker interactions are to be expected. As the parameter d changes, different values of the SIF at the main crack tip are realised, amplified or shielded according to the value of the parameter itself.

For each of the three kinds of geometries, various samples are obtained imposing the sequence of values 0.5, 1.0, 1.5 and 2.0 to the parameter h/l. For each of these values, the horizontal spacing S_0 was given the dimensions of two, three and four times the microcrack half-length. In this way the most disperse microcrack array was obtained for $h/l = 2.0$ and $S_0/l = 4.0$, while the most strongly interacting array corresponds to the geometry defined by $h/l = 0.5$ and $S_0/l = 2.0$. This set of twelve geometries is considered for each of the three kinds of microcrack arrays (a), (b) and (c), Figure 14.

The distance d is given several values inside a range defined as the interval in which the microcracks have any noticeable effect over the main crack, with a scanning step not higher than 0.1 in dimensionless units, corresponding to 5 percent of the microcrack full-length. This range depends on the number of microcracks composing the array, widening as the microcracks are increased in their number. In this way the diagrams $K_I/K_{I0} - 1$ versus d/l are plotted, with a number of numerical simulations varying from 200 up to 350 for each diagram.

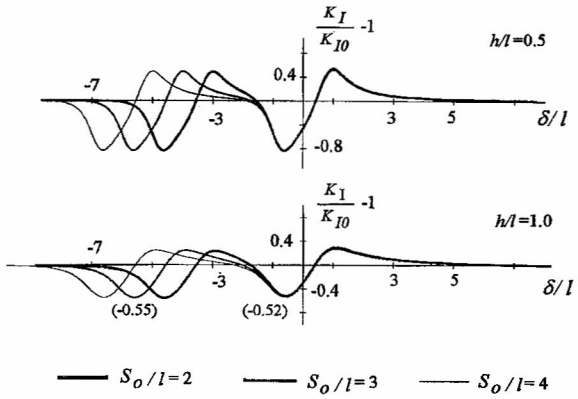

Figure 15. Diagrams for the 8 microcrack geometry, $h/l = 0.5, h/l = 1.0$.

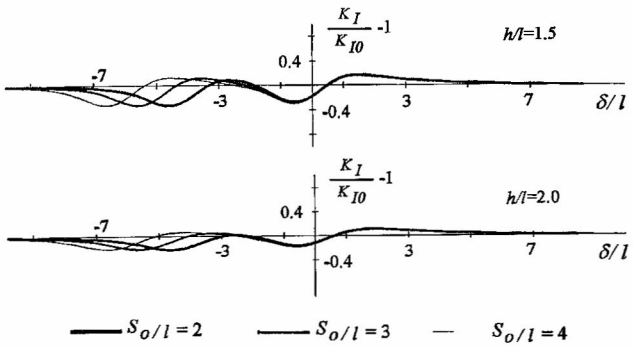

Figure 16. Diagrams for the 8 microcrack geometry, $h/l = 1.5, h/l = 2.0$.

Figures 15 and 16 present the twelve diagrams for the geometry with eight microcracks, while Figures 17 and 18 present the same series for the 18 microcrack geometry.

Figures 19, 20 and 21 refer to the 56 microcrack geometry and present analogous diagrams for, respectively, horizontal spacings equal to two, three and four times the microcrack half-length.

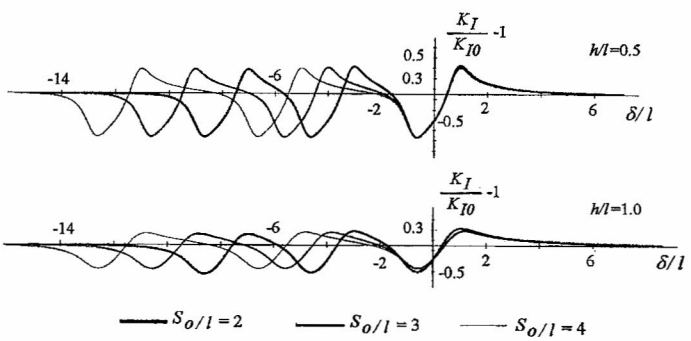

Figure 17. Diagrams for the 18 microcrack geometry, $h/l = 0.5, h/l = 1.0$.

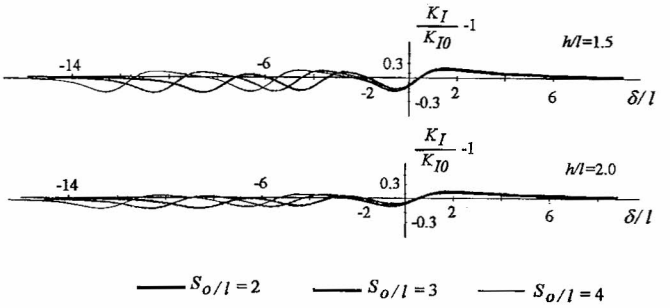

Figure 18. Diagrams for the 18 microcrack geometry, $h/l = 1.5, h/l = 2.0$.

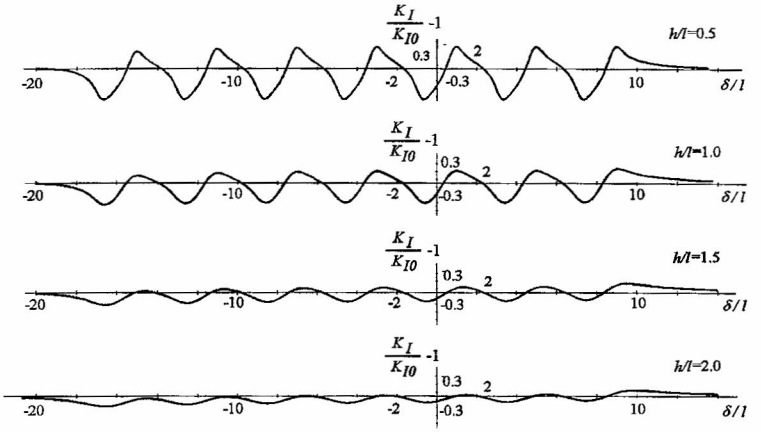

Figure 19. Fifty-six microcrack array, $S_0/l = 2$.

9. Discussion of the numerical results

The comparison of the diagrams with the same vertical spacing h/l – for all three geometries presented in Figure 14 – shows that the horizontal spacing has little influence on the phenomenon.

The diagrams have a number of relative minimums and maximums coincident with the number of columns, corresponding each maximum (minimum) to the position of the micro-

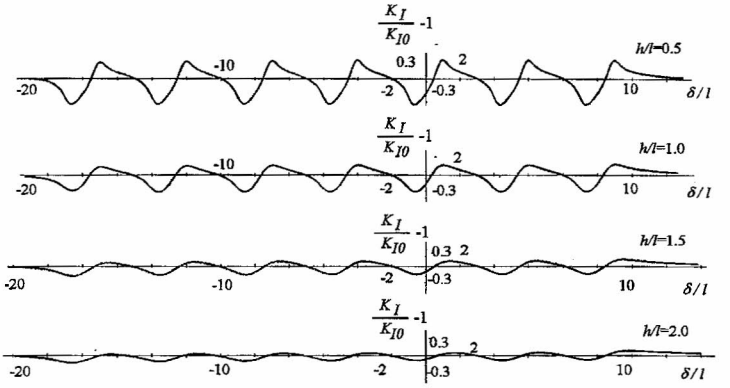

Figure 20. Fifty-six microcrack array, $S_0/l = 3$.

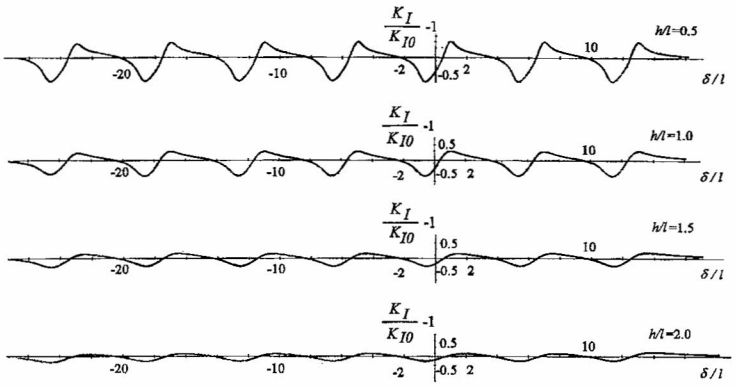

Figure 21. Fifty-six microcrack array, $S_0/l = 4$.

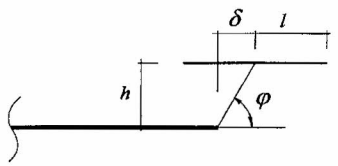

Figure 22. Angle between the horizontal line and a segment joining the main crack tip and the centre of the closest microcrack.

crack array in which a single column has the main role in the amplification (shielding) phenomenon. These peak values, in fact, change as the horizontal spacing is increased, but the absolute variation of the values is hardly significant. As the columns of microcracks are more dispersed (higher S_0) the maximums get lower values, since the other microcrack columns in front of the main crack tip are more distant and thus can give a weaker contribution in amplifying the SIF of the main crack. In the same way, consistent variations of the maximum shielding effects can be found. For example, in the eight microcrack geometry (Figures 15 and 16), for $h/l = 1$, when all the microcracks are located in front of the main crack (all the microcracks having amplifying effects) the maximum shielding effect is some 3 percent weaker than in the other shielding position in which the first column of microcracks is located in the *wake region* and thus cannot contribute to the amplification of the SIF at the main crack tip. In any case, the influence of this parameter is of somewhat low importance.

Changing the vertical spacing h is of much greater effect. As the parameter h/l increases, both the amplification and shielding effects rapidly decrease in magnitude; the diagrams remain asymmetric but the peak values are so quickly cut down that a vertical distance h equal to 2.5 times the microcrack half-length can be considered the limit for negligible interactions.

In each kind of geometry there is a '*neutral position*', identified by values of the front distance d/l in the range [0.3, 0.8], in which the SIF at the main crack tip is the same as that for the undamaged material. Computing the angle between an horizontal line and a segment joining the main crack tip and the centre of the closest microcrack (Figure 22) the values of Table 1 are obtained for $S_0/l = 3$.

While the angle φ is about seventy degrees for the three sets of geometries having $h/l = 1.0, 1.5$ and 2.0, it is important to point out that strong interaction $(h/l = 0.5)$ lowers this angle to about fifty degrees.

Analogous considerations can be made for the position of relative maximum obtainable for values of the parameter d/l in the range [1, 2]. Table 2 summarises the angles, as defined

Table 1. Angles corresponding to the neutral positions for $S_0/l = 3$

h/l	2 microcracks	8 microcracks	18 microcracks	56 microcracks
0.5	$\varphi = 47°$	$\varphi = 51°$	$\varphi = 47°$	$\varphi = 50°$
1.0	$\varphi = 63°$	$\varphi = 69°$	$\varphi = 71°$	$\varphi = 72°$
1.5	$\varphi = 68°$	$\varphi = 72°$	$\varphi = 74°$	$\varphi = 71°$
2.0	$\varphi = 68°$	$\varphi = 73°$	$\varphi = 75°$	$\varphi = 70°$

Table 2. Angles corresponding to the maximum amplification for $S_0/l = 3$

h/l	2 microcracks	8 microcracks	18 microcracks	56 microcracks
0.5	$\varphi = 27°$	$\varphi = 27°$	$\varphi = 27°$	$\varphi = 27°$
1.0	$\varphi = 41°$	$\varphi = 45°$	$\varphi = 42°$	$\varphi = 45°$
1.5	$\varphi = 45°$	$\varphi = 47°$	$\varphi = 45°$	$\varphi = 49°$
2.0	$\varphi = 47°$	$\varphi = 48°$	$\varphi = 45°$	$\varphi = 47°$

in Figure 22, for which the maximum amplification is found. As previously found for the maximum shielding configurations, the strongest interactions are related to geometries characterized by an angle for the maximum amplification which is substantially smaller than the angle of the other geometries.

On the contrary, the maximum shielding position is obtained always for a frontal distance d/l equal to -0.6, corresponding, case by case, to the angles reported in Table 3. This fact points out an outstanding consideration: amplification and shielding cannot be considered as symmetrical phenomena, they are in some way different.

The diagrams of Figure 23 are obtained considering the absolute maximum and minimum values of the SIF at the main crack tip for $S_0/l = 2$, varying h/l. It can be seen that the maximum shielding is almost untouched by the number of microcracks, and can therefore be considered a short-range effect. The maximum amplification, on the other hand, is significantly altered by the number of microcracks so much that, for $h/l = 2.0$, the amplification due to fifty-six microcracks is almost twice the one due to two microcracks.

10. Results and conclusions

The numerical technique proposed, based on displacement discontinuity boundary elements, proved to be efficient to take into account the interactions between cracks, giving high precision also in rather challenging cases. At the expense of reasonable computational efforts, many general cases were dealt with, for which the only requirement is a preliminary study on the

Table 3. Angles corresponding to the maximum shielding for $S_0/l = 3$.

h/l	0.5	1.0	1.5	2.0
φ	140°	121°	112°	107°

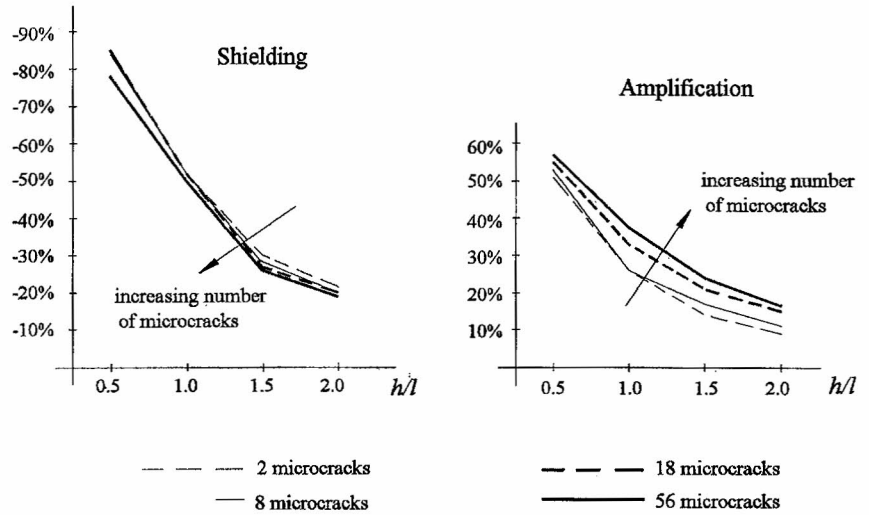

Figure 23. Maximum amplification and shielding as function of the vertical spacing and microcrack number for $S_0/l = 2$.

mesh refinement for elementary cases. The results were found to be mesh-independent to a satisfactory extent.

The boundary element technique herein proposed postulates that the displacements along the crack are constant in certain intervals, being allowed a parabolic deformation near the tips. The '*pseudo-traction method*' [12] assumes instead that the stress acting on the crack line can be considered as constant, which is a good approximation only for weakly interacting cracks. When the distance between cracks is so short that a strong interaction is expected, then the '*pseudo-traction method*' looses precision, as shown by some comparisons. The present boundary element method allows a detailed analysis up to very close distances.

The displacement discontinuity procedure outlined in Section 2 significantly differs from other boundary element techniques. Some hybrid boundary element codes [20] require the plate to be modelled as a finite plate of huge dimensions (not less than twenty-five times the main crack length) by fictitious stress elements [17], while the crack could be modelled by displacement discontinuity elements. This brings about a higher computational effort and a lack of precision, particularly when strong interactions take place.

The pure displacement discontinuity procedure described in the present paper overcomes these drawbacks, allowing analysis in infinite plates, as well as in finite plates, with a somewhat higher precision.

Crack interaction is usually considered a short range phenomenon involving only a few of the closest microcracks. This was found to be true to some extent only for shielding of the main crack which seems to be almost unaffected by the number of microcracks (Figure 23). On the contrary, the amplification of the SIF at the main crack tip is significantly altered by far located microcracks. Thus amplification has to be considered a phenomenon characterised by a range which is wider than the shielding range, as confirmed also by other authors through a double layer potential technique [19]. In addition, the difference found in the angles for maximum shielding or maximum amplification geometries underlines the asymmetry between the two phenomena.

Describing the position of the microcrack arrays which produce the maximum shielding or amplification effects through a polar coordinate system, and in particular through the angle φ (Figure 22) it was found that when the interaction is weak, the inclination φ is the same for all three cases, while, when the interaction is stronger, the inclination is significantly different. A deeper insight into the phenomenon is likely needed.

In some materials, like ceramics, damage is modelled by means of random microcrack distributions [15, 21, 22] located in front of the main crack. Experimental investigations [1] show that this process zone is quite long in front of the main crack tip. The results presented in this paper go further in this direction, giving some reasons for taking into account distant microcracks, the interaction of which has been found to be not negligible *a priori*.

Acknowledgements

The authors gratefully acknowledge the financial support of the National Research Council (CNR) and the Department for University and Scientific and Technological Research (MURST).

References

1. L.X. Han and S. Suresh, High-temperature failure of an Alumina-Silicon Carbide composite under cyclic loads: mechanisms of fatigue crack tip damage, *Journal of the American Ceramic Society* 72 (1989) 1233–1238.
2. J.W. Hutchinson, Crack tip shielding by micro-cracking in brittle solids, *Acta Metallurgica* 35 (1987) 1609–1619.
3. M. Ruhle, A.G. Evans, R.M. McMeeking, P.G. Charalambides and J.W. Hutchinson, Microcrack toughening in Alumina/Zirconia, *Acta Metallurgica* 35 (1987) 2701–2710.
4. W. Kreher and W. Pompe, Increased fracture toughness of ceramics by energy-dissipative mechanisms, *Journal of Material Science* 16 (1981) 694–706.
5. D.R. Clarke, A simple calculation of process-zone toughening by microcracking, *Commentaries of the American Ceramic Society*, January 1984, C-15, C-16.
6. L.R. Rose, Microcrack interaction with a main crack, *International Journal of Fracture* 31 (1986) 233–242.
7. A.A. Rubinstein, Macrocrack interaction with semi-infinite microcrack array, *International Journal of Fracture* 27 (1985) 113–119.
8. A.A. Rubinstein and H.C. Choi, Macrocrack interaction with transverse array of microcracks, *International Journal of Fracture* 36 (1988) 15–26.
9. H. Horii and S. Nemat-Nasser, Elastic fields of interacting inhomogeneities, *International Journal of Solids and Structures* 21 (1985) 731–745.
10. S. Gong and H. Horii, General solution to the problem of microcracks near the tip of a main crack, *Journal of Mechanics and Physics of Solids* 37 (1989) 27–46.
11. K.Y. Lam, C. Wen and Z. Phua, Interaction between microcracks and a main crack in a semi-infinite medium, *Engineering Fracture Mechanics* 44 (1993) 753–761.
12. M. Kachanov, Elastic solids with many cracks: a simple method of analysis, *International Journal of Solids and Structures* 23 (1987) 23–43.
13. M. Kachanov and E. Montagut, Interaction of a crack with certain microcrack arrays, *Engineering Fracture Mechanics* 25 (1986) 625–636.
14. P.G. Charambides and R.M. McMeeking, Finite element method simulation of a crack propagation in a brittle microcracked solid, *Mechanics of Materials* 6 (1987) 71–87.
15. X. Huang and B.L. Karihaloo, Interaction of penny shaped cracks with a half plane crack, *International Journal of Solids and Structures* 25 (1993) 591–607.
16. S.L. Crouch, Solution of plane elasticity problems by the displacement discontinuity method: I Infinite body solution; II Semi-infinite body solution, *International Journal for Numerical Methods in Engineering* 10 (1976) 301–343.
17. S.L. Crouch and A.M. Starfield, *Boundary Element Methods in Solid Mechanics*, Unwin Hyman, Cambridge (1983).
18. A. Carpinteri, *Mechanical Damage and Crack Growth in Concrete*, Martinus Nijhoff Publishers, Dordrecht (1986).

19. A. Dolgopolsky, V. Karbhari and S.S. Kwak, Microcrack induced toughening – an interaction model, *Acta Metallurgica* 37 (1989) 1349–1354.
20. C. Scavia, A numerical technique for the analysis of cracks subjected to normal compressive stresses, *International Journal for Numerical Methods in Engineering* 33 (1992) 929–942.
21. J.P. Laures and M. Kachanov, Three dimensional interactions of a crack front with arrays of penny-shaped microcracks, *International Journal of Fracture* 48 (1991) 255–279.
22. A. Brencich, A. Carpinteri and C. Scavia, Disorder effects on the interaction between a main crack and a distribution of microcracks, *Journal of Applied Mechanics (ASME)*, submitted for publication.